Photoacoustics 37 (2024) 100595

Contents lists available at ScienceDirect

Photoacoustics

journal homepage: www.elsevier.com/locate/pacs

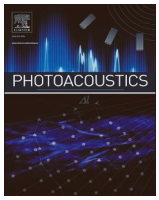

A mini-resonant photoacoustic sensor based on a sphere-cylinder coupled acoustic resonator for high-sensitivity trace gas sensing

Guojie Wu [a], Yongjia Zhang [b], Zhenfeng Gong [a,*], Yeming Fan [a], Jiawei Xing [b], Xue Wu [b], Junsheng Ma [a], Wei Peng [c], Qingxu Yu [a], Liang Mei [a,*]

[a] School of Optoelectronic Engineering and Instrumentation Science, Dalian University of Technology, Dalian 116024, Liaoning, China
[b] School of Dalian University of Technology and Belarusian State University Joint Institute, Dalian University of Technology, Dalian, Liaoning 116024, China
[c] School of Physics, Dalian University of Technology, Dalian 116024, Liaoning, China

ARTICLE INFO

Keywords:
Mini-resonant photoacoustic sensor
Sphere-cylinder coupled photoacoustic resonator
Trace gas sensing

ABSTRACT

This paper reports a mini-resonant photoacoustic sensor for high-sensitivity trace gas sensing. The sensor primarily contains a sphere-cylinder coupled acoustic resonator, a cylindrical buffer chamber, and a fiber-optic acoustic sensor. The acoustic field distributions of this mini-resonant photoacoustic sensor and the conventional T-type resonant photoacoustic sensor have been carefully evaluated, showing that the first-order resonance frequency of the present mini-resonant photoacoustic sensor is reduced by nearly a half compared to that of the T-type resonant photoacoustic sensor. The volume of the developed photoacoustic cavity is only about 0.8 cm^3. Trace methane is selected as the target analytical gas and a detection limit of 101 parts-per-billion at 100-s integration time has been achieved, corresponding to a normalized noise equivalent absorption (NNEA) coefficient of 1.04×10^{-8} $W \cdot cm^{-1} \cdot Hz^{-1/2}$. The developed mini-resonant photoacoustic sensor provides potential for high-sensitivity trace gas sensing in narrow spaces.

1. Introduction

Trace gas sensing is of great significance in the areas of medical diagnosis [1,2], combustion diagnostic [3], environmental monitoring [4,5], fire alarm [6], etc. Laser-based photoacoustic spectroscopy (PAS) has been successfully implemented for ultra-sensitive trace gas sensing in recent years [7–21]. The photoacoustic effect is that the modulated light source is absorbed resulting in periodic heating of the gas in a photoacoustic cell (PAC), generating acoustic waves that can be detected by a microphone [22–25]. Hence, the performance of the microphone and the PAC has an important impact on the detection sensitivity of a PAS system. Recently, quartz tuning fork acoustic sensors [26–32] based on the electrical detection method and fiber-optic acoustic sensors [33–39] based on the optical detection method have been successfully implemented in PAS systems, featuring high sensitivity and small size.

In recent years, the PAC, as one of the key components affecting the performance of the PAS sensing system, has gained a lot of attention [40]. Based on the operating modes of the PAC, it can be categorized into non-resonant and resonant PACs [41]. Compared with the non-resonant PACs, the resonant PACs are more widely used for trace gas detection due to their higher sensitivity and higher signal-to-noise ratio (SNR). The H-type resonant PAC (HR-PAC), featuring easy processing and good symmetry, has been frequently utilized in PAS for trace gas measurements [42]. Wang *et al.* designed and proposed an all-optical PAS system to detect trace acetylene gases by integrating a fiber-optic microphone into the HR-PAC [43]. The detection limit was 1.56 parts per billion (ppb) (SNR = 1) for a 1 s integration time. In 2020, Gong *et al.* optimized the dimensional relationship between buffer cavities and acoustic resonator of an HR-PAC to obtain a higher photoacoustic signal [44]. The final detection limit of nitrogen dioxide (NO_2) reached 1.26 ppb. To further improve the detection limit, Yin *et al.* used a differential HR-PAC, two condenser microphones, and a blue multimode diode laser (optical power: 3.5 W) to construct a PAS system for trace NO_2 sensing [45]. A detection limit of 54 parts per trillion (ppt) was achieved for an integration time of 1 s. In 2022, Zhao *et al.* showed a highly sensitive CH_4 photoacoustic sensor based on a differential multi-pass HR-PAC [46]. With an integral time of 1 s, the corresponding detection limit and the normalized noise equivalent absorption (NNEA) coefficient were 19.9 ppb and 1.79×10^{-10} $cm^{-1} \cdot W \cdot Hz^{-1/2}$, respectively. However, the HR-PAC typically consists of two buffer chambers and one or two

* Corresponding authors.
E-mail addresses: gongzf@dlut.edu.cn (Z. Gong), meiliang@dlut.edu.cn (L. Mei).

https://doi.org/10.1016/j.pacs.2024.100595
Received 20 November 2023; Received in revised form 15 January 2024; Accepted 7 February 2024
Available online 9 February 2024

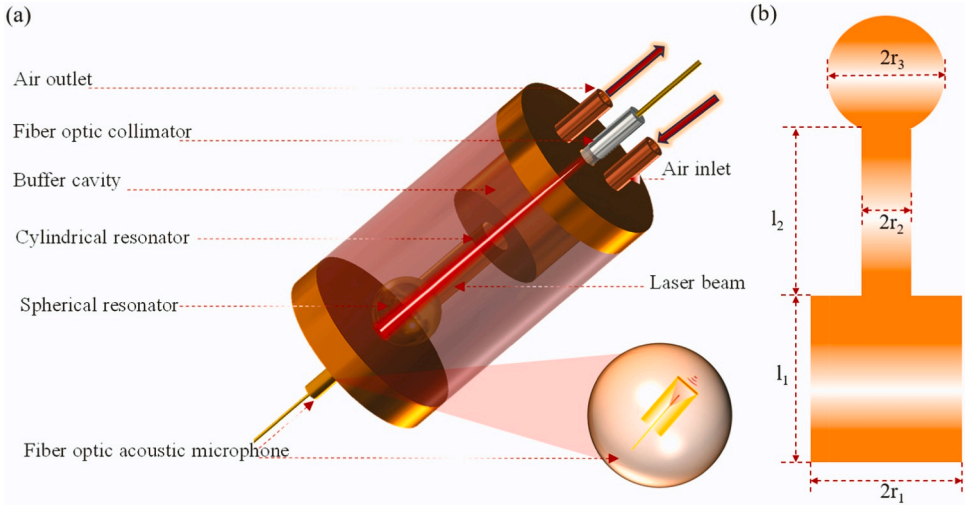

Fig. 1. (a) The sketch of the mini-resonant photoacoustic sensor (b) the mechanical schematic diagram of the photoacoustic cavity.

resonators. As a result, the volume of the HR-PAC is large, leading to a relatively longer response time during gas measurements.

In order to obtain a resonant PAC with a smaller volume and higher performance, Gong *et al.* reported a T-type resonant PAC (TR-PAC), which mainly consisted of a buffer volume, and a resonator [35]. Compared with the HR-PAC, the TR-PAC featured a higher photoacoustic signal, a smaller volume, a larger cell constant. In 2022, Xiao *et al.* introduced an ultra-high sensitivity all-optical differential PAS sensor, primarily composed of two fiber-optic microphones and a two-channel differential TR-PAC, which had a sub-ppb detection limit for methane (CH_4) [36]. In 2023, Zhou *et al.* reported a miniature dual-resonance PAS sensor based on a piezoelectric ceramics slice and a miniature TR-PAC [47]. The volume of the entire sensor was reduced by optimizing the size of the TR-PAC's resonator and buffer chamber. Finally, the sensor volume was only 3.75 cm^3. The natural resonant frequencies of the piezoelectric ceramic slice and the TR-PAC were designed to be 8280 Hz and 8350 Hz, respectively, to obtain the double resonance effect. The sensor had a detection limit of 15 ppm for CH_4 gas with an integral time of 10 s. Although the newly reported miniature dual-resonance PAS sensor had a small size, the operating frequency of this sensor was placed at a high frequency (8350 Hz), resulting in a low photoacoustic signal and thus a poorer detection limit. Thus, there is a trade-off between a small-size resonant PAC and a high photoacoustic signal.

This paper proposes a novel mini-resonant photoacoustic sensor with mini-resonant PAC but much higher photoacoustic signal, compared with the traditional TR-PAC-based sensor. The acoustic field distributions of both the mini-resonant photoacoustic sensor and the traditional TR-PAC-based sensor have been simulated. A laser-based PAS system, employing the mini-resonant photoacoustic sensor as the detection unit, a 1650.96 nm distributed feedback laser (DFB) as the excitation unit, and a high-speed spectrometer as the demodulation unit, has been developed to validate the performance of the mini-resonant photoacoustic sensor.

2. Sensor structure and simulation analysis

The sketch of the mini-resonant photoacoustic sensor is shown in Fig. 1(a), mainly including a fiber-optic collimator, a buffer cavity, a sphere-cylinder coupled acoustic resonator, a fiber-optic acoustic microphone, an air inlet, and an air outlet. The collimator has a diameter of 1.8 mm and a working distance of 120 mm. Fig. 1(b) presents the mechanical schematic diagram of the photoacoustic cavity. The buffer cavity has a dimension of 5 mm (r_1) × 8 mm (l_1). The cylindrical acoustic resonator has a dimension of 1.5 mm (r_2) × 8 mm(l_2). The 3D models of

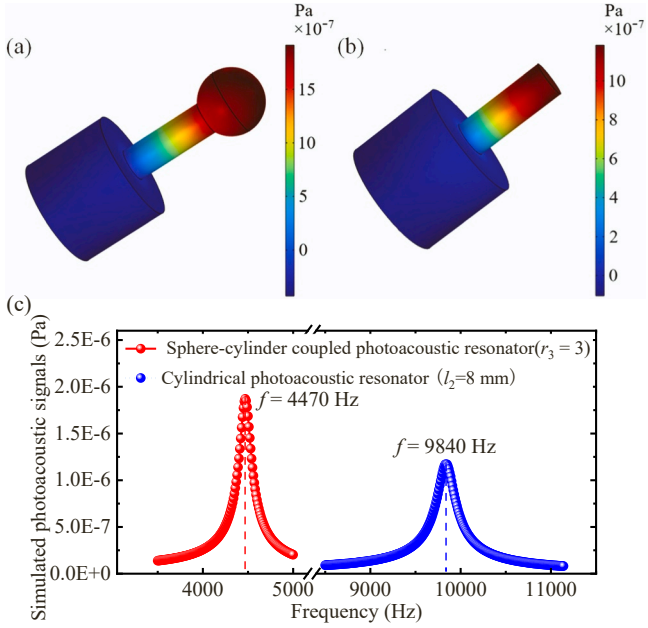

Fig. 2. The acoustic pressure field cloud maps of (a) the sphere-cylinder coupled resonator (b) the cylindrical resonator at their resonant frequencies. (c) The corresponding simulated frequency response curves of the two acoustic resonators.

the cylindrical resonator and the sphere-cylinder coupled resonator are developed by utilizing the finite element analysis method based on COMSOL Multiphysics software. The simulation model mainly employs the pressure acoustics module in the acoustic physics field. The thermo-adhesive boundary layer in the acoustic module is also utilized to make the simulated frequency response results consistent with the actual application scenarios. The scanning ranges of the resonant frequency are set at 3500–5000 Hz for the cylindrical resonator and 8500–11140 Hz for the sphere-cylinder coupled resonator, with a frequency step of 10 Hz. Fig. 2(a) and (b) depict the acoustic pressure field cloud maps of the two types of resonators at their resonant frequencies, respectively. As can be seen from Fig. 2(a) and (b), the acoustic pressure field cloud maps of both PACs demonstrate that the resonator end is the antinode position of the photoacoustic signal. Thus, a fiber-optic acoustic sensor is placed here to detect the maximum photoacoustic signal amplitude. In addition, the corresponding simulated frequency response curves of the

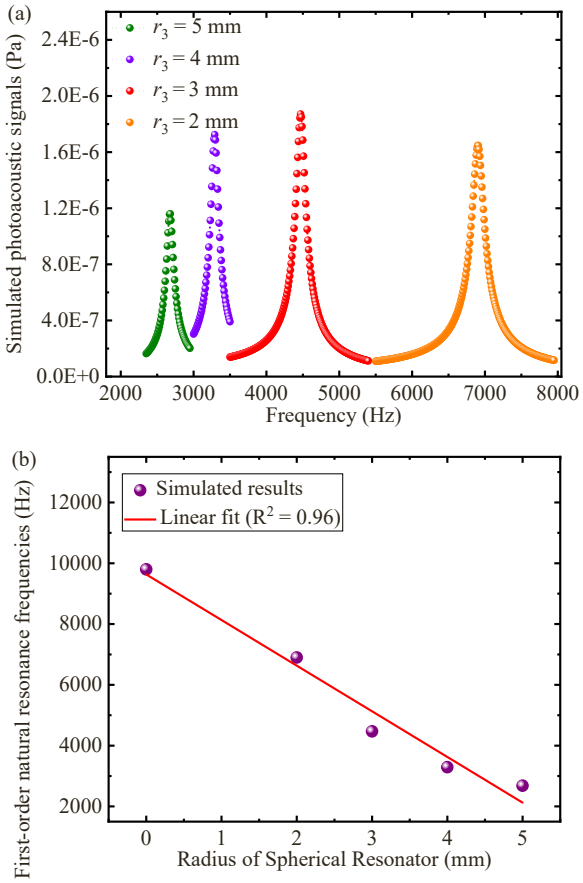

Fig. 3. (a) The simulated frequency response curves for sphere-cylinder coupled acoustic resonators with spherical radii of 2 mm, 3 mm, 4 mm and 5 mm. (b) The first-order resonance frequencies as a function of the spherical radius of the sphere-cylinder coupled acoustic resonator.

two acoustic resonators are described in Fig. 2(c). The simulated resonance frequency of the cylindrical resonator of TR-PAC is 9840 Hz, while the simulated resonance frequency of the sphere-cylinder coupled resonator is only about a half, i.e., 4470 Hz.

Numerical simulation has been carried out to further analyze the influence of different spherical radii of the sphere-cylinder coupled acoustic resonator on the first-order resonance frequency and photoacoustic signals. The simulated frequency response curves for the sphere-cylinder coupled acoustic resonator with radii of 2 mm, 3 mm, 4 mm and 5 mm are shown in Fig. 3. As the increasing of the spherical radius, the first-order resonance frequency decreases while the amplitude of the photoacoustic signal first increases and then decreases. Moreover, when the spherical radius of the sphere-cylinder coupled acoustic resonator is 3 mm, the amplitude of the photoacoustic signal is maximum. Fig. 3(b) depicts the relationship between first-order resonance frequency and the spherical radius of the sphere-cylinder coupled acoustic resonator, where a R^2 value of 0.96 has been achieved, showing that the first-order resonance frequency and the spherical radius of the sphere-cylinder coupled acoustic resonator have a good linear relationship. Considering the performance of the sensor, as well as the sampling frequency of the spectrometer, the spherical radius(r_3) of the sphere-cylinder coupled acoustic resonator is chosen to be 3 mm. The sensor is fabricated by 3D printing technology using a photosensitive resin with a manufacturing precision of 0.2 mm.

3. Experiments and results

3.1. Instrumentation

Fig. 4(a) depicts the schematic of the experimental configuration to detect CH_4 with the high-performance mini-resonant photoacoustic sensor. A distributed feedback laser diode is employed as the light source for CH_4 absorption measurements with a center wavelength of 1650.96 nm. The simulation results of the absorption coefficients of 1 ppm CH_4, and 5000 ppm H_2O from 1650.2 nm to 1660 nm bands obtained through the HITRAN 2012 database are plotted in Fig. 4(b). Under this absorption line, the absorption coefficient of 1 ppm CH_4 is 2–3 orders of magnitude higher than that of 5000 ppm H_2O and 1000 ppm CO_2. Thus, choosing this center wavelength (1650.96 nm) as the absorption line for CH_4 avoids the influence of H_2O and CO_2 on the response of the target gas. A super-luminescent diode (SLD), with a center wavelength of 1550 nm and a spectral width of 60 nm, is served as the broadband probe light. A high-speed spectrometer with 512 pixels in total and a line frequency of up to 5 kHz is used to sample the interference spectrum. The mixed concentrations of CH_4 and pure nitrogen (N_2) are controlled by two mass flow controllers. The DFB laser diode generates a laser beam first passing through a fiber-optic collimator (120-mm working distance at 1650.96 nm), and then injecting into the mini-resonant photoacoustic sensor without contacting with the

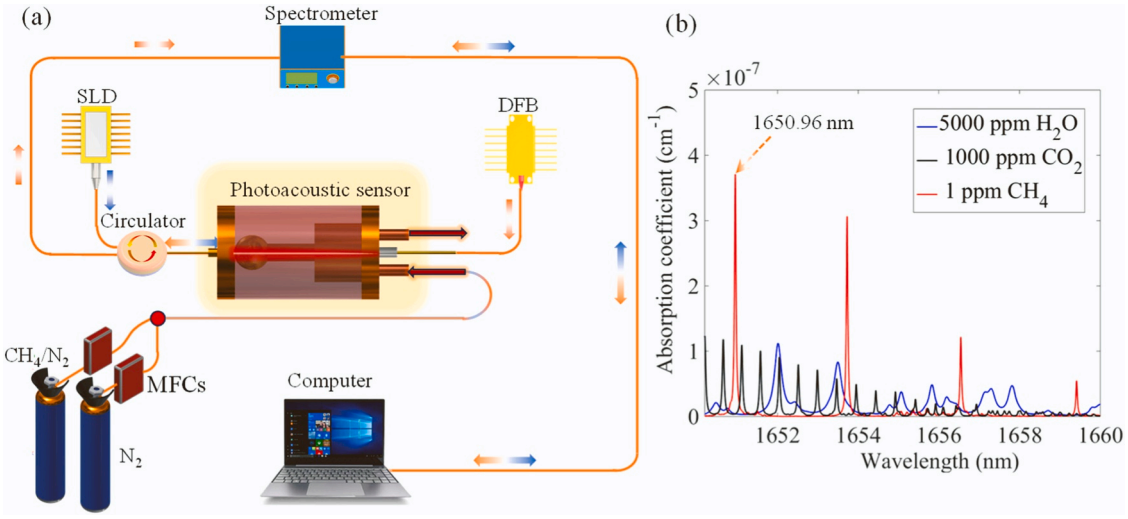

Fig. 4. (a) The schematic of the experimental configuration to detect CH_4 with the mini-resonant photoacoustic sensor. (b) Absorption coefficients of 1 ppm CH_4, 5000 ppm H_2O and 1000 ppm CO_2 from 1650.2 nm to 1660 nm.

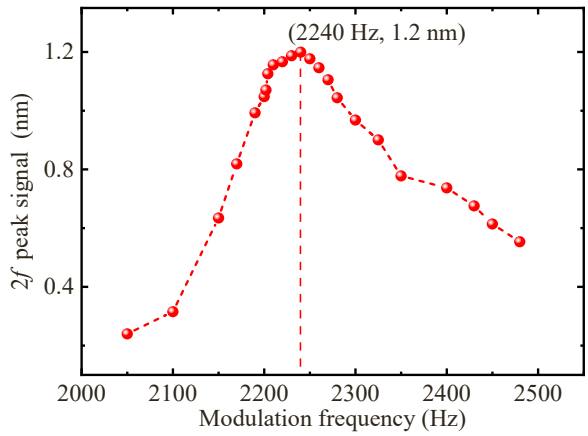

Fig. 5. The experiment frequency response curve of the mini-resonant photoacoustic sensor obtained by changing the modulation frequency from 2050 Hz to 2500 Hz.

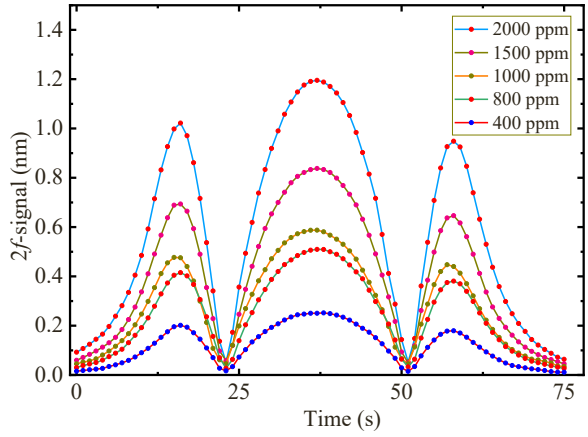

Fig. 6. The WMS-2*f* scans spectra of CH_4 (400–2000 ppm).

side wall of the PAC. The absorption of the pump light by CH_4 gas leads to the periodic release of heat and thus to the production of photoacoustic signal, which forces the vibration of the fiber-optic microphone. The broadband probe light generated by the SLD is injected into the Fabry-Perot cavity of the fiber-optic microphone through a circulator, and the corresponding interference spectrum are received by the high-speed spectrometer and demodulated by a digital lock-in amplifier to acquire the photoacoustic signal.

3.2. *Performance testing of the designed photoacoustic sensor*

The sample gas with a CH_4 concentration of 2000 ppm is filled into the mini-resonant photoacoustic sensor to verify the first-order resonance frequency of the designed PAC. The temperature and the bias current of the DFB laser are set to 25 ℃ and 63.9 mA to obtain the maximum photoacoustic signal. The wavelength-modulated spectroscopy (WMS) technique is employed to capture the photoacoustic signal [48]. The experiment frequency response curve of the mini-resonant photoacoustic sensor obtained by changing the modulation frequency from 2050 Hz to 2500 Hz is presented in Fig. 5. The maximum 2 *f* signal appears at a modulation frequency of 2240 Hz. Therefore, the first-order resonance frequency of the PAC is 4480 Hz, which is basically consistent with the simulation results shown in Fig. 2. Finally, the experimental modulation frequency is fixed at 2240 Hz.

A 2000 ppm CH_4 gas is mixed with pure N_2 through mass flow controllers to obtain CH_4 sample gases with different concentrations

Table 1
The means and standard deviations corresponding to different gas concentrations.

Gas concentration (ppm)	Average value (nm)	Standard deviation (nm)
2000	1.193	0.016
1500	0.827	0.0178
1000	0.600	0.017
800	0.48814	0.01177
400	0.26512	0.01343

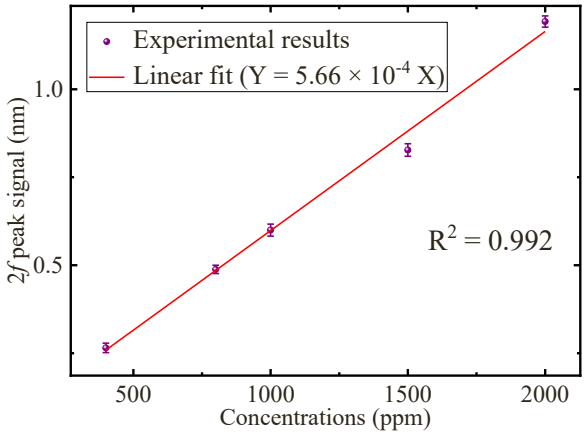

Fig. 7. The means and standard deviations of the peak WMS-2*f* signal with different CH_4 concentrations.

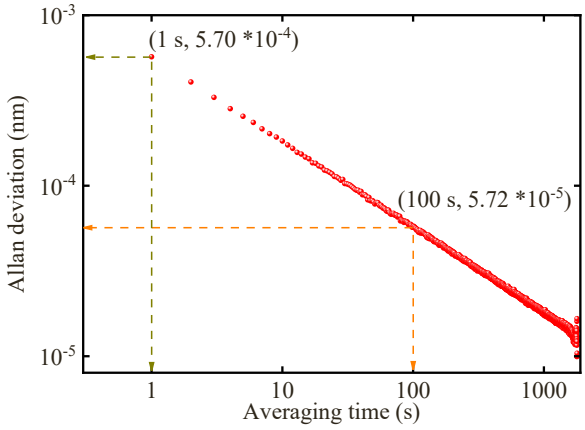

Fig. 8. The Allan-Werle deviation.

(400–2000 ppm). The sample gases are passed into the photoacoustic sensor to test the sensitivity and linear response of the designed sensor. Fig. 6 exhibits the measured WMS-2*f* scan spectra with different CH_4 concentrations. The means and standard deviations of the 2 *f* peak signals for different CH_4 concentrations are obtained are obtained as shown in the Table 1. For each gas concentration the corresponding standard deviation is less than 0.02 nm, which shows that the designed photoacoustic sensor has good repeatability, high accuracy and excellent stability during the test. Fig. 7 shows the means and standard deviations of the peak WMS-2*f* signal with different CH_4 concentrations. The sensitivity of the mini-resonant photoacoustic sensor for CH_4 is 5.66×10^{-4} nm/ppm. The *R*-squared value can reach up to 0.992, showing excellent linear response to CH_4 gases.

An Allan-Werle deviation [49–53] analysis has been performed to evaluate the detection limit of the sensor and long-term stability. When the temperature, the modulation current, and the modulation frequency

Table 2
A comparison of the performance with other PAS CH_4 sensors.

PAC operating mode	Laser wavelength (nm)	Cavity volume (cm^3)	Detection limit @ IT (ppb)	NNEA ($W•cm^{-1}•Hz^{1/2}$)	Ref.
Non-resonate	1650.96	1.1×10^{-3}	51100 @ 1 s	4.57×10^{-7}	[13]
Non-resonate	1650.96	4.19	1230 @ 1 s	not stated	[25]
Resonate	1653.7	267.8	1800 @ 183 s	2.7×10^{-9}	[40]
Resonate	1645.61	3.75	15750 @ 10 s	not stated	[47]
Resonate	1650.96	222	200 @ 400 s	2.9×10^{-9}	[54]
Resonate	1650.96	186.83	430 @ 1 s	9.75×10^{-9}	[55]
Resonate	3311	9.1	14930 @ 1 s	2.2×10^{-7}	[56]
Resonate	**1650.96**	**0.8**	**1000 @ 1 s**	**10.4×10^{-9}**	**[This paper]**

of the laser are set to 25 ℃, 63.9 mA, and 2240 Hz, respectively, the WMS-2*f* peak signals are continuously measured and recorded. The Allan-Werle deviation is obtained, as shown in Fig. 8. The detection limit of the mini-resonant photoacoustic sensor, is found to be 1 ppm for CH_4 with a 1-s integration time, the corresponding noise level is 5.7×10^{-4} nm and the sensitivity is 5.66×10^{-4} nm/ppm. Furthermore, when the integration time is extended to 100 s, the noise level is further reduced to 5.72×10^{-5} nm, and the corresponding detection limit is inferred to be 101 ppb. The NNEA can reach up to 1.04×10^{-8} $W \cdot cm^{-1} \cdot Hz^{-1/2}$ with a 1-s integration time (0.25 Hz bandwidth), when the output power of the DFB laser diode is 14 mW.

The simulation analysis and experimental results demonstrate that the developed mini-resonant photoacoustic sensor has a high performance while maintaining a volume of less than 1 cubic centimeter. Benefiting from the integrated design of the spherical and cylindrical resonators, the mini-resonant photoacoustic sensor has a superior detection sensitivity and a relatively lower first-order resonance frequency compared to the conventional T-resonance PAC-based sensor. To further demonstrate the characteristics of the developed sensor, Table 1 summarizes the performances of various CH_4 photoacoustic gas sensors reported in recent years. It can be seen from Table 1 that the present mini-resonant photoacoustic sensor has a small cavity volume while maintaining comparable or even superior sensitivity and NNEA compared to the PAS sensors operating in resonant and non-resonant modes. Table 2.

4. Conclusions

In this work, a novel high-performance mini-resonant photoacoustic sensor for trace gas sensing is proposed, which primarily consists of a sphere-cylinder coupled acoustic resonator, a cylindrical buffer chamber, and a fiber-optic acoustic sensor. The acoustic field distributions of this mini-resonant photoacoustic sensor and the T-type resonant PAS sensor are analyzed by using COMSOL, indicating that the first-order resonance frequency of this mini-resonant photoacoustic sensor is reduced by nearly a half compared to the conventional T-type resonant PAS sensor. In addition, the influence of the radius of the spherical resonator on the resonance frequency and photoacoustic signal have been systematically analyzed through numerical simulations. The radius of the spherical resonator is finally determined to be 3 mm. The volume of the developed photoacoustic cavity is only about 0.8 cm^3. Trace CH_4 is the target analytical gas, and the detection limit is 1 ppm at 1-s integration time, corresponding to an NNEA coefficient of 1.04×10^{-8} $W \cdot cm^{-1} \cdot Hz^{-1/2}$, which can be further improve by prolonging the integration time. The proposed PAS sensor demonstrates superior performances compared to the previously developed resonant and non-resonant PAS sensors, and provides a new scheme for high-sensitivity miniaturized PAS-based trace gas sensing. Meanwhile, the performance of the developed mini-resonant photoacoustic CH_4 sensor might be further improved by utilizing a near-infrared Raman fiber optic amplifier, a mid-infrared laser source, or an optical frequency comb light source.

Funding

This work was supported by National Natural Science Foundation of China [grant numbers 62075025]; Natural Science Foundation of Liaoning Province [grant numbers 2022-MS-127]; Fundamental Research Funds for the Central Universities [grant numbers DUT22-LAB102, DUT22JC17, DUT22QN246].

CRediT authorship contribution statement

Yu Qingxu: Writing – review & editing. **Wu Guojie:** Writing – original draft, Software, Data curation, Conceptualization. **Zhang Yongjia:** Visualization, Resources, Data curation. **Mei Liang:** Writing – review & editing, Writing – original draft, Supervision. **Xing Jiawei:** Software, Resources. **Wu Xue:** Software, Resources. **Gong Zhenfeng:** Writing – review & editing, Supervision. **Fan Yeming:** Methodology, Investigation. **Ma Junsheng:** Methodology, Investigation. **Peng Wei:** Supervision.

Declaration of Competing Interest

The authors declare that they have no known competing financial interests or personal relationships that could have appeared to influence the work reported in this paper.

Data availability

Data will be made available on request.

References

[1] M. Jahjah, W. Ren, P. Stefański, R. Lewicki, J. Zhang, W. Jiang, J. Tarka, F.K. Tittel, A compact QCL based methane and nitrous oxide sensor for environmental and medical applications, Analyst 139 (2014) 2065–2069, https://doi.org/10.1039/C3AN01452E.
[2] X. Mao, P. Zheng, X. Wang, S. Yuan, Breath methane detection based on all-optical photoacoustic spectrometer, Sens. Actuators B Chem. 239 (2017) 1257–1260, https://doi.org/10.1016/j.snb.2016.09.132.
[3] W. Ren, A. Farooq, D. Davidson, R. Hanson, CO concentration and temperature sensor for combustion gases using quantum-cascade laser absorption near 4.7 μm, Appl. Phys. B. 107 (2012), https://doi.org/10.1007/s00340-012-5046-1.
[4] I. Bamberger, J. Stieger, N. Buchmann, W. Eugster, Spatial variability of methane: Attributing atmospheric concentrations to emissions, Environ. Pollut. 190 (2014) 65–74, https://doi.org/10.1016/j.envpol.2014.03.028.
[5] E.G. Nisbet, E.J. Dlugokencky, P. Bousquet, Atmospheric science. Methane on the rise-again, Science 343 (2014) 493–495, https://doi.org/10.1126/science.1247828.
[6] J.L. Bradshaw, J.D. Bruno, K.M. Lascola, R.P. Leavitt, J.T. Pham, F.J. Towner, D. M. Sonnenfroh, K.R. Parameswaran, Small low-power consumption CO-sensor for post-fire cleanup aboard spacecraft, Proc. SPIE 8032 (2011) 80320D, https://doi.org/10.1117/12.887517.
[7] G. Wu, Z. Gong, H. Li, J. Ma, K. Chen, W. Peng, Q. Yu, L. Mei, High-Sensitivity Multitrace Gas Simultaneous Detection Based on an All-Optical Miniaturized Photoacoustic Sensor, Anal. Chem. 94 (2022) 12507–12513, https://doi.org/10.1021/acs.analchem.2c02767.
[8] M.E. Webber, M. Pushkarsky, C.K.N. Patel, Fiber-amplifier-enhanced photoacoustic spectroscopy with near-infrared tunable diode lasers, Appl. Opt. 42 (12) (2003) 2119–2126, https://doi.org/10.1364/AO.42.002119.
[9] W. Jin, Y. Cao, F. Yang, H.L. Ho, Ultra-sensitive all-fiber photothermal spectroscopy with large dynamic range, Nat. Commun. 6 (2015) 6767, https://doi.org/10.1038/ncomms7767.

[10] C. Zhang, S. Qiao, Y. Ma, Highly sensitive photoacoustic acetylene detection based on differential photoacoustic cell with retro-reflection-cavity, Photoacoustics 30 (2023) 100467, https://doi.org/10.1016/j.pacs.2023.100467.
[11] L. Zhang, L. Liu, X. Zhang, X. Yin, H. Huan, H. Liu, X. Zhao, Y. Ma, X. Shao, T-type cell mediated photoacoustic spectroscopy for simultaneous detection of multi-component gases based on triple resonance modality, Photoacoustics 31 (2023) 100492, https://doi.org/10.1016/j.pacs.2023.100492.
[12] X. Zhao, M. Guo, D. Cui, C. Li, H. Qi, K. Chen, F. Ma, J. Huang, G. Zhang, J. Zhao, Multi-pass differential photoacoustic sensor for real-time measurement of SF_6 decomposition component H_2S at the ppb level, Anal. Chem. 95 (2023) 8214–8222, https://doi.org/10.1021/acs.analchem.3c00003.
[13] Z. Gong, G. Wu, K. Chen, M. Guo, J. Ma, H. Li, F. Ma, L. Mei, W. Peng, Q. Yu, Fiber-Tip Gas Transducer Based on All-Optical Photoacoustic Spectroscopy, J. Light. Technol. 40 (2022) 5300–5306, https://doi.org/10.1109/JLT.2022.3171524.
[14] M. Olivieri, M. Giglio, S. Dello Russo, G. Menduni, A. Zifarelli, P. Patimisco, A. Sampaolo, H. Wu, L. Dong, V. Spagnolo, Assessment of vibrational-translational relaxation dynamics of methane isotopologues in a wet-nitrogen matrix through QEPAS, Photoacoustics 31 (2023) 100518, https://doi.org/10.1016/j.pacs.2023.100518.
[15] X. Liu, H. Wu, L. Dong, Methodology and applications of acousto-electric analogy in photoacoustic cell design for trace gas analysis, Photoacoustics 30 (2023) 100475, https://doi.org/10.1016/j.pacs.2023.100475.
[16] Z. Gong, T. Gao, L. Mei, K. Chen, Y. Chen, B. Zhang, W. Peng, Q. Yu, Ppb-level detection of methane based on an optimized T-type photoacoustic cell and a NIR diode laser, Photoacoustics 21 (2021) 100216, https://doi.org/10.1016/j.pacs.2020.100216.
[17] Y. Cao, W. Jin, H.L. Ho, J. Ma, Miniature fiber-tip photoacoustic spectrometer for trace gas detection, Opt. Lett. 38 (4) (2013) 434–436, https://doi.org/10.1364/OL.38.000434.
[18] B. Chen, H. Li, X. Zhao, M. Gao, K. Cheng, X. Shao, H. Wu, L. Dong, X. Yin, Trace photoacoustic SO_2 gas sensor in SF_6 utilizing a 266 nm UV laser and an acousto-optic power stabilizer, Opt. Express 31 (2023) 6974–6981, https://doi.org/10.1364/OE.483240.
[19] B. Li, H. Wu, C. Feng, J. Wang, S. Jia, P. Zheng, L. Dong, Photoacoustic Heterodyne CO Sensor for Rapid Detection of CO Impurities in Hydrogen, Anal. Chem. 96 (2024) 547–553, https://doi.org/10.1021/acs.analchem.3c04753.
[20] G. Wu, J. Xing, Z. Gong, J. Ma, Y. Fan, X. Wu, W. Peng, Q. Yu, L. Mei, Single fiber-type double cavity enhanced photoacoustic spectroscopy sensor for trace methane sensing, J. Light. Technol. (2024), https://doi.org/10.1109/JLT.2024.3353200.
[21] R. Cui, H. Wu, F.K. Tittel, V. Spagnolo, W. Chen, L. Dong, Folded-optics-based quartz-enhanced photoacoustic and photothermal hybrid spectroscopy, Photoacoustics 35 (2024) 100580, https://doi.org/10.1016/j.pacs.2023.100580.
[22] G. Wu, Z. Gong, J. Ma, H. Li, M. Guo, K. Chen, W. Peng, Q. Yu, L. Mei, High-sensitivity miniature dual-resonance photoacoustic sensor based on silicon cantilever beam for trace gas sensing, Photoacoustics 27 (2022) 100386, https://doi.org/10.1016/j.pacs.2022.100386.
[23] H. Wu, L. Dong, H. Zheng, Y. Yu, W. Ma, L. Zhang, W. Yin, L. Xiao, S. Jia, F. K. Tittel, Beat frequency quartz-enhanced photoacoustic spectroscopy for fast and calibration-free continuous trace-gas monitoring, Nat. Commun. 8 (2017) 15331, https://doi.org/10.1038/ncomms15331.
[24] M. Olivieri, G. Menduni, M. Giglio, A. Sampaolo, P. Patimisco, H. Wu, L. Dong, V. Spagnolo, Characterization of H_2S QEPAS detection in methane-based gas leaks dispersed into environment, Photoacoustics 29 (2023) 100438, https://doi.org/10.1016/j.pacs.2022.100438.
[25] Y. Jiao, H. Fan, Z. Gong, K. Yang, F. Shen, K. Chen, L. Mei, W. Peng, Q. Yu, Trace CH_4 Gas Detection Based on an Integrated Spherical Photoacoustic Cell, Appl. Sci. 11 (2021) 4997, https://doi.org/10.3390/app11114997.
[26] A.A. Kosterev, Y.A. Bakhirkin, R.F. Curl, F.K. Tittel, Quartz-enhanced photoacoustic spectroscopy, Opt. Lett. 27 (2002) 1902–1904, https://doi.org/10.1364/OL.27.001902.
[27] H. Lin, C. Wang, L. Lin, M. Wang, W. Zhu, Y. Zhong, J. Yu, F. Tittel, H. Zheng, Non-contact quartz-enhanced photoacoustic spectroscopy, Appl. Phys. Lett. 122 (2023) 111101, https://doi.org/10.1063/5.0134744.
[28] C. Zhang, S. Qiao, Y. He, S. Zhou, L. Qi, Y. Ma, Differential quartz-enhanced photoacoustic spectroscopy, Appl. Phys. Lett. 122 (2023) 241103, https://doi.org/10.1063/5.0157161.
[29] A. Sampaolo, P. Patimisco, L. Dong, A. Geras, G. Scamarcio, T. Starecki, F.K. Tittel, V. Spagnolo, Quartz-enhanced photoacoustic spectroscopy exploiting tuning fork overtone modes, Appl. Phys. Lett. 107 (2015) 231102, https://doi.org/10.1063/1.4937002.
[30] M. Olivieri, G. Menduni, M. Giglio, A. Sampaolo, P. Patimisco, H. Wu, L. Dong, V. Spagnolo, Characterization of H_2S QEPAS detection in methane-based gas leaks dispersed into environment, Photoacoustics 29 (2023) 100438, https://doi.org/10.1016/j.pacs.2022.100438.
[31] G. Menduni, A. Zifarelli, A. Sampaolo, P. Patimisco, M. Giglio, N. Amoroso, H. Wu, L. Dong, R. Bellotti, V. Spagnolo, High-concentration methane and ethane QEPAS detection employing partial least squares regression to filter out energy relaxation dependence on gas matrix composition, Photoacoustics 26 (2022) 100349, https://doi.org/10.1016/j.pacs.2022.100349.
[32] Y. Ma, Y. Hu, S. Qiao, Z. Lang, X. Liu, Y. He, V. Spagnolo, Quartz tuning forks resonance frequency matching for laser spectroscopy sensing, Photoacoustics 25 (2022) 100329, https://doi.org/10.1016/j.pacs.2022.100329.
[33] Y. Yin, D. Ren, C. Li, R. Chen, J. Shi, Cantilever-enhanced photoacoustic spectroscopy for gas sensing: A comparison of different displacement detection methods, Photoacoustics 28 (2022) 100423, https://doi.org/10.1016/j.pacs.2022.100423.
[34] M. Guo, K. Chen, B. Yang, G. Zhang, X. Zhao, C. Li, Miniaturized anti-interference cantilever-enhanced fiber-optic photoacoustic methane sensor, Sens. Actuators B Chem. 370 (2022) 132446, https://doi.org/10.1016/j.snb.2022.132446.
[35] Z. Gong, K. Chen, Y. Chen, L. Mei, Q. Yu, Integration of T-type half-open photoacoustic cell and fiber-optic acoustic sensor for trace gas detection, Opt. Express 27 (2019) 18222–18231, https://doi.org/10.1364/OE.27.018222.
[36] H. Xiao, J. Zhao, C. Sima, P. Lu, Y. Long, Y. Ai, W. Zhang, Y. Pan, J. Zhang, D. Liu, Ultra-sensitive ppb-level methane detection based on NIR all-optical photoacoustic spectroscopy by using differential fiber-optic microphones with gold-chromium composite nanomembrane, Photoacoustics 26 (2022) 100353, https://doi.org/10.1016/j.pacs.2022.100353.
[37] Z. Gong, Y. Chen, T. Gao, K. Chen, Y. Jiao, M. Guo, B. Zhang, S. Liu, L. Mei, W. Peng, Q. Yu, Parylene-C diaphragm-based low-frequency photoacoustic sensor for space-limited trace gas detection, Opt. Lasers Eng. 134 (2020) 106288, https://doi.org/10.1016/j.optlaseng.2020.106288.
[38] Z. Gong, K. Chen, Y. Yang, X. Zhou, Q. Yu, Photoacoustic spectroscopy based multi-gas detection using high-sensitivity fiber-optic low-frequency acoustic sensor, Sens. Actuators B Chem. 260 (2018) 357–363, https://doi.org/10.1016/j.snb.2018.01.005.
[39] L. Fu, P. Lu, C. Sima, J. Zhao, Y. Pan, T. Li, X. Zhang, D. Liu, Small-volume highly-sensitive all-optical gas sensor using non-resonant photoacoustic spectroscopy with dual silicon cantilever optical microphones, Photoacoustics 27 (2022) 100382, https://doi.org/10.1016/j.pacs.2022.100382.
[40] Y. Wei, Q. Huang, J. Li, Dual-gas detection based on high-performance spherical photoacoustic cells, Sens. Actuators A Phys. 360 (2023) 114542, https://doi.org/10.1016/j.sna.2023.114542.
[41] V.A. Kapitanov, V. Zeninari, B. Parvitte, D. Courtois, Yu.N. Ponomarev, Optimisation of photoacoustic resonant cells with commercial microphones for diode laser gas detection, Spectrochim. Acta A. 58 (2002) 2397–2404, https://doi.org/10.1016/S1386-1425(02)00054-9.
[42] R.A. Rooth, A.J. Verhage, L.W. Wouters, Photoacoustic measurement of ammonia in the atmosphere: influence of water vapor and carbon dioxide, Appl. Opt. 29 (1990) 3643–3653, https://doi.org/10.1364/AO.29.003643.
[43] Q. Wang, J. Wang, L. Li, Q. Yu, An all-optical photoacoustic spectrometer for trace gas detection, Sens. Actuators B Chem. 153 (2011) 214–218, https://doi.org/10.1016/j.snb.2010.10.035.
[44] Z. Gong, T. Gao, Y. Chen, B. Zhang, W. Peng, Q. Yu, F. Ma, L. Mei, K. Chen, Sub-ppb level detection of nitrogen dioxide based on an optimized H-type longitudinal acoustic resonator and a lock-in white-light interferometry demodulation algorithm, J. Quant. Spectrosc. Ra 253 (2020) 107136, https://doi.org/10.1016/j.jqsrt.2020.107136.
[45] X. Yin, L. Dong, H. Wu, H. Zheng, W. Ma, L. Zhang, W. Yin, S. Jia, F. Tittel, Sub-ppb nitrogen dioxide detection with a large linear dynamic range by use of a differential photoacoustic cell and a 3.5W blue multimode diode laser, Sens. Actuators B Chem. 247 (2017), https://doi.org/10.1016/j.snb.2017.03.058.
[46] X. Zhao, K. Chen, D. Cui, M. Guo, C. Li, H. Qi, G. Zhang, Z. Gong, Z. Zhou, W. Peng, Ultra-high sensitive photoacoustic gas detector based on differential multi-pass cell, Sens. Actuators B Chem. 368 (2022) 132124, https://doi.org/10.1016/j.snb.2022.132124.
[47] J. Zhou, P. Gong, L. Xie, Z. Er, Y. chang, X. Jiang, Y. Wang, A new design method for miniature dual-resonance photoacoustic structure based on piezoelectric ceramics slice, Infrared Phys. Techn. (2023) 104849, https://doi.org/10.1016/j.infrared.2023.104849.
[48] L. Mei, S. Svanberg, Wavelength modulation spectroscopy-digital detection of gas absorption harmonics based on Fourier analysis, Appl. Opt. 54 (2015) 2234–2243, https://doi.org/10.1364/AO.54.002234.
[49] P.O. Werle, R. Mücke, F. Slemr, The limits of signal averaging in atmospheric trace-gas monitoring by tunable diode-laser absorption spectroscopy (TDLAS), Appl. Phys. B 57 (2) (1993) 131–139, https://doi.org/10.1007/BF00425997.
[50] B. Zhang, Y. Jia, B. Zhao, X. Zhu, Y. Shi, Highly sensitive photoacoustic gas sensor with micro-embedded acoustic resonator for gas leakage detection, Opt. Lett. 48 (2023) 4201–4204, https://doi.org/10.1364/OL.497052.
[51] Y. Zhang, Y. Xie, J. Lu, J. Zhao, Y. Wu, J. Tong, J. Shao, Continuous real-time monitoring of carbon dioxide emitted from human skin by quartz-enhanced photoacoustic spectroscopy, Photoacoustics 30 (2023) 100488, https://doi.org/10.1016/j.pacs.2023.100488.
[52] H. Wu, X. Yin, L. Dong, K. Pei, A. Sampaolo, P. Patimisco, H. Zheng, W. Ma, L. Zhang, W. Yin, L. Xiao, V. Spagnolo, S. Jia, F.K. Tittel, Simultaneous dual-gas QEPAS detection based on a fundamental and overtone combined vibration of quartz tuning fork, Appl. Phys. Lett. 110 (2017) 121104, https://doi.org/10.1063/1.4979085.
[53] H. Wu, L. Dong, H. Zheng, X. Liu, X. Yin, W. Ma, L. Zhang, W. Yin, S. Jia, F.K. Tittel, Enhanced near-infrared QEPAS sensor for sub-ppm level H2S detection by means of a fiber amplified 1582nm DFB laser, Sens. Actuators B Chem. 221 (2015) 666–672, https://doi.org/10.1016/j.snb.2015.06.049.
[54] K. Liu, J. Mei, W. Zhang, W. Chen, X. Gao, Multi-resonator photoacoustic spectroscopy, Sens. Actuators B Chem. 251 (2017) 632–636, https://doi.org/10.1016/j.snb.2017.05.114.
[55] Y. Li, G. Guan, Y. Lu, X. Liu, S. Yang, C. Zheng, F. Song, Y. Zhang, Y. Wang, F. K. Tittel, Highly sensitive near-infrared gas sensor system using a novel H-type resonance-enhanced multi-pass photoacoustic cell, Measurement 220 (2023) 113380, https://doi.org/10.1016/j.measurement.2023.113380.
[56] Y. Chen, T. Liang, S. Qiao, Y. Ma, A Miniaturized 3D-Printed Quartz-Enhanced Photoacoustic Spectroscopy Sensor for Methane Detection with a High-Power Diode Laser, Sensors 23 (2023) 4034, https://doi.org/10.3390/s23084034.

Guojie Wu is currently working towards his master degree at the School of Optoelectronic Engineering and Instrumentation Science, Dalian University of Technology (DUT). His research interest is photoacoustic spectroscopy and deep learning.

Yongjia Zhang is currently working towards his master degree at School of Dalian University of Technology and Belarusian State University Joint Institute, Dalian University of Technology (DUT). His research interest is photoacoustic spectroscopy and fiber optic sensing.

Zhenfeng Gong received his Ph.D. degree in optical engineering from the Dalian University of Technology (DUT), Dalian, China, in 2018. He is currently a lecture in the School of Optoelectronic Engineering and Instrumentation, DUT. His current research interests include fiber-optic sensors and photoacoustic spectroscopy.

Yeming Fan is currently working towards his master degree at the School of Optoelectronic Engineering and Instrumentation Science, Dalian University of Technology (DUT). His research interest is photoacoustic spectroscopy and deep learning.

JiaweiXing is currently working towards his master degree at School of Dalian University of Technology and Belarusian State University Joint Institute, Dalian University of Technology (DUT). His research interest is photoacoustic spectroscopy and deep learning.

XueWu is currently working towards his master degree at School of Dalian University of Technology and Belarusian State University Joint Institute, Dalian University of Technology (DUT). His research interest is photoacoustic spectroscopy.

Junsheng Ma is currently working towards his master degree at the School of Optoelectronic Engineering and Instrumentation Science, Dalian University of Technology (DUT). His research interest is photoacoustic spectroscopy and Distributed fiber optic sensing.

Wei Peng is currently a professor at the School of Optoelectronic Engineering and Instrumentation Science, at Dalian University of Technology. Her current research interests are fiber-optic sensors, micro / nano photonics and surface plasmon resonance.

Qingxu Yu is currently a professor at the School of Optoelectronic Engineering and Instrumentation Science, at Dalian University of Technology. His current research interests are fiber-optic sensors and laser spectroscopy.

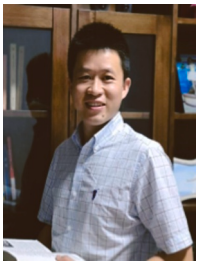

Liang Mei obtained his PhD from Zhejiang University in 2013 and then from Lund University in 2014 with independent research topics. He is now affiliated with the School Optoelectronic Engineering and Instrumentation Science, Dalian University of Technology, where he has been active as an associate professor since 2015. His research interests concern applications of laser spectroscopy to environmental, biophotonics, and food safety fields.